Neuron
Article

Proprioceptive Coupling within Motor Neurons Drives *C. elegans* Forward Locomotion

Quan Wen,[1,*] Michelle D. Po,[3] Elizabeth Hulme,[2] Sway Chen,[1] Xinyu Liu,[2] Sen Wai Kwok,[2] Marc Gershow,[1] Andrew M. Leifer,[1] Victoria Butler,[4,5] Christopher Fang-Yen,[1,6] Taizo Kawano,[3] William R. Schafer,[4] George Whitesides,[2] Matthieu Wyart,[7] Dmitri B. Chklovskii,[5] Mei Zhen,[3] and Aravinthan D.T. Samuel[1,*]
[1]Department of Physics and Center for Brain Science
[2]Department of Chemistry
Harvard University, Cambridge, MA 02138, USA
[3]Samuel Lunenfeld Research Institute, Mount Sinai Hospital, Toronto, ON M5G 1X5, Canada
[4]MRC Laboratory of Molecular Biology, University of Cambridge, Cambridge CB2 0QH, UK
[5]Janelia Farm Research Campus, HHMI, Ashburn, VA 20147, USA
[6]Department of Bioengineering, University of Pennsylvania, Philadelphia, PA 19104, USA
[7]Department of Physics, New York University, New York, NY 10003, USA
*Correspondence: vineygeyser@gmail.com (Q.W.), samuel@physics.harvard.edu (A.D.T.S.)
http://dx.doi.org/10.1016/j.neuron.2012.08.039

SUMMARY

Locomotion requires coordinated motor activity throughout an animal's body. In both vertebrates and invertebrates, chains of coupled central pattern generators (CPGs) are commonly evoked to explain local rhythmic behaviors. In *C. elegans*, we report that proprioception within the motor circuit is responsible for propagating and coordinating rhythmic undulatory waves from head to tail during forward movement. Proprioceptive coupling between adjacent body regions transduces rhythmic movement initiated near the head into bending waves driven along the body by a chain of reflexes. Using optogenetics and calcium imaging to manipulate and monitor motor circuit activity of moving *C. elegans* held in microfluidic devices, we found that the B-type cholinergic motor neurons transduce the proprioceptive signal. In *C. elegans*, a sensorimotor feedback loop operating within a specific type of motor neuron both drives and organizes body movement.

INTRODUCTION

All locomotory circuits, from invertebrates to limbed vertebrates, must generate rhythmic activities throughout their motor systems (Delcomyn, 1980; Grillner, 2003; Marder and Calabrese, 1996). To exhibit coherent gaits such as crawling, walking, swimming, or running, the rhythmic activities of all body parts must be patterned in specific temporal sequences (Delcomyn, 1980; Grillner, 2003; Marder and Calabrese, 1996; Mullins et al., 2011). Rhythmic motor activities are typically generated by dedicated neural circuits with intrinsic rhythmic activities called the central pattern generators (CPG) (Brown, 1911; Delcomyn, 1980; Grillner, 2003; Kiehn, 2011; Marder and Calabrese, 1996; Mullins et al., 2011). Networks of CPGs can be distributed throughout a locomotory circuit. For example, chains of CPGs have been identified along the nerve cord of the leech, and distributed CPG modules have also been found in mammalian lumbar spinal cord to control hindlimb movement (Kiehn, 2006). In isolated nerve cords or spinal cords, even after all muscle and organ tissues have been removed, motor circuits that correspond to different body parts generate spontaneous rhythmic activity, a fictive resemblance of the swimming patterns in behaving animals (Cohen and Wallén, 1980; Kristan and Calabrese, 1976; Mullins et al., 2011; Pearce and Friesen, 1984; Wallén and Williams, 1984).

When a chain of CPGs generates autonomous rhythmic activities, where each CPG corresponds to a different body part, mechanisms to coordinate their activities must be present. Sensory feedback often plays a critical role in this coordination (Grillner and Wallén, 2002; Mullins et al., 2011; Pearson, 1995, 2004). In lamprey and leech, for example, specialized proprioceptive neurons in the spinal cord and body wall modulate the spontaneous activity of CPGs within each body segment (Cang and Friesen, 2000; Cang et al., 2001; Grillner et al., 1984). Activation of these stretch-sensitive neurons, either by current injection or by externally imposed body movements, can entrain CPG activity (McClellan and Jang, 1993; Yu and Friesen, 2004). Similarly, in limbed vertebrates, sensory feedback from mechanoreceptors in the skin and muscle, working through interneuronal circuits that modulate the rhythmic bursting of motor neurons, helps to coordinate limb movements during step cycles (Pearson, 2004).

Here, we study undulatory wave propagation along the body of the nematode *Caenorhabditis elegans* during forward movement (Figure 1A). The worm offers an opportunity to obtain a complete systems-level understanding of a locomotory circuit. The adult motor circuit has been mapped at synaptic resolution (Chen et al., 2006; White et al., 1986). Recent advances in optical neurophysiology (Chronis et al., 2007; Clark et al., 2007; Faumont et al., 2011; Guo et al., 2009; Haspel et al., 2010; Kawano et al., 2011; Leifer et al., 2011; Liewald et al., 2008; Zhang et al., 2007) now make it possible to explore the physiology of this motor circuit in freely moving animals.

C. elegans locomotion is controlled by a network of excitatory cholinergic (A- and B-types) and inhibitory GABAergic (D-type)

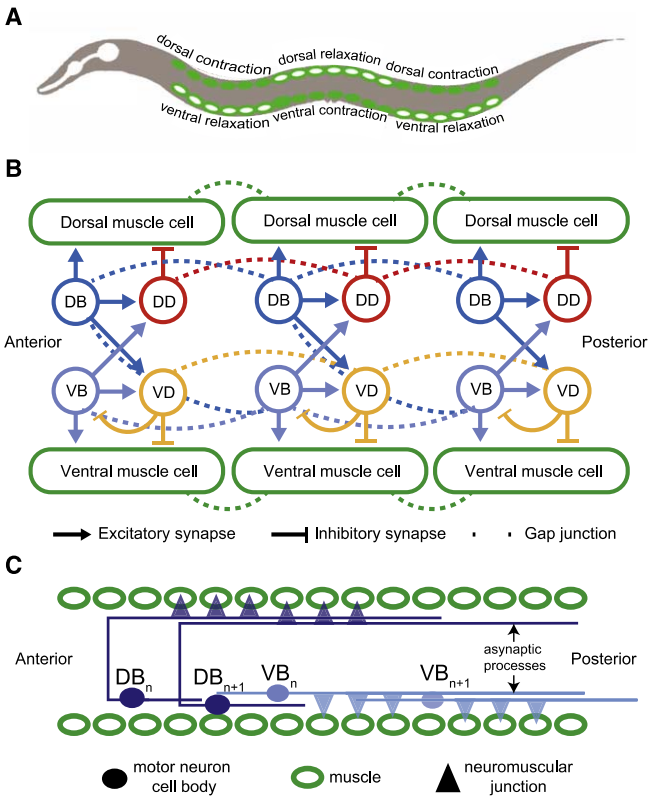

Figure 1. A Schematic Diagram of the Motor Circuit in *C. elegans*

(A) Worms undulate by alternating contraction and relaxation of dorsal and ventral muscle cells lining the body. Dorsal bending is achieved when dorsal muscle cells contract (filled cells) and ventral muscle cells relax (open cells). Ventral bending is achieved when ventral muscle cells contract and dorsal muscle cells relax.

(B) General patterns of connectivity in the wiring diagram for forward movement. Arrows indicate excitatory chemical synapses from the cholinergic motor neurons (VB and DB). Blunt-ended lines indicate inhibitory chemical synapses from GABAergic motor neurons (DD and VD). GABAergic neurons are dispensable for the propagation of the bending wave along the worm body during forward movement. Dashed lines indicate gap junctions between neighboring muscle cells and neighboring neurons of each cell type. Six to twelve neurons of each cell type are distributed along the worm body. The schematic diagram is based on Chen (2007), Durbin (1987), Haspel and O'Donovan (2011), and White et al. (1986).

(C) The morphology of DB and VB motor neurons along the circuit. All cell bodies are located in the ventral nerve cord. The axons of VB motor neurons have short anterior axons and long posterior axons. The axons of the DB motor neurons cross to the dorsal nerve cord with long posterior projections. See also Figure S6.

motor neurons along the nerve cord that innervate the muscle cells lining the worm body (White et al., 1976). Earlier cell ablation studies suggest that B-type cholinergic motor neurons are specifically required for forward locomotion in L1 larva (Chalfie et al., 1985). The 11 VB and 7 DB neurons innervate the ventral and dorsal musculature, respectively (Figure 1). The A-type cholinergic motor neurons, which are necessary for backward movement (Chalfie et al., 1985), are similarly divided into the D and V subclasses that innervate the dorsal and ventral musculature (not shown in Figure 1).

How the *C. elegans* motor circuit organizes bending waves along its body during locomotion is poorly understood. Even when all premotor interneurons are ablated (Kawano et al., 2011; Zheng et al., 1999), *C. elegans* retains the ability to generate local body bending, suggesting that the motor circuit itself (A-, B-, and D-type neurons and muscle cells) can generate undulatory waves. However, the synaptic connectivity of the motor circuit does not contain motifs that might be easily interpreted as local CPG elements that could spontaneously generate oscillatory activity (e.g., oscillators driven by mutual inhibition between two neuronal classes that can be found in larger animals) (Figure 1B). The synaptic connectivity does contain a pattern to avoid simultaneous contraction of both ventral and dorsal muscles; the VB and DB motor neurons that activate the ventral and dorsal muscles also activate the opposing inhibitory GABAergic motor neurons (DD and VD, respectively). However, this contralateral inhibition generated by GABAergic neurons is not essential for rhythmic activity along the body or the propagation of undulatory waves during forward locomotion (McIntire et al., 1993).

In addition, unlike in larger animals, the *C. elegans* motor circuit does not contain specialized proprioceptive or mechanosensory afferents that are positioned to provide information about local movements to each body region through local sensory or interneurons (Figure 1B). The DVA interneuron has been shown to have proprioceptive properties (Hu et al., 2011; Li et al., 2006), but its process spans the whole worm body and is not required for forward locomotion. The lack of specialized sensory neurons within the motor circuit led Russell and Byerly to speculate that individual motor neurons might themselves have proprioceptive properties (White et al., 1986). In particular, electron microscopy showed that the cholinergic motor neurons have long undifferentiated processes that extend along the nerve cord without making synapses. In the B-type motor neurons, for example, these long asynaptic processes extend farther posteriorly than do their neuromuscular junctions (Figure 1C) (White et al., 1986). These asynaptic processes were hypothesized to represent specialized proprioceptive sensors. If this is the case, proprioceptive information might be expected to travel from posterior to anterior in the B-type motor neurons. A putative mechanosensory channel, UNC-8, is also expressed in motor neurons (Tavernarakis et al., 1997). However, whether any motor neuron is capable of proprioception, or how proprioception is used by the motor circuit, has not been demonstrated.

Biomechanical evidence also implies a role for proprioception in *C. elegans* locomotion as its gait adapts to the mechanical load imposed by the environment (Berri et al., 2009; Boyle et al., 2012; Fang-Yen et al., 2010). When worms swim in low-load environments, such as water, the bending wave has a long wavelength (~1.5 body length *L*). When crawling or swimming in high-load environments ~10,000-fold more viscous than water, the bending wave has a short wavelength (~0.65 *L*), but whether or how proprioception might be related to gait adaptation has not been determined.

Here, we examined whether the worm motor circuit has proprioceptive properties and how these properties are connected to undulatory dynamics. We apply microfluidic devices and in vivo optical neurophysiology to show that proprioceptive coupling between adjacent body segments constitutes the trigger that

drives bending wave propagation from head to tail. We found that posterior body regions are compelled to bend in the same direction and shortly after the bending of the neighboring anterior region. We localize this form of proprioceptive coupling to the B-type cholinergic motor neurons. We quantify the spatial and temporal dynamics of this proprioceptive coupling, and use our biophysical measurements to calculate its role in undulatory dynamics. Proprioception in the *C. elegans* motor circuit, beyond simply explaining the propagation of an undulatory wave from head to tail, also provides a quantitative explanation for gait adaptation to external load.

RESULTS

The Bending of One Body Region Requires the Bending of Its Anterior Neighbor

C. elegans moves forward on its side by propagating dorsal-ventral body bending waves from head to tail. The detailed kinematics of bending waves can be quantified by measuring curvature κ at each point along the body centerline over time (Figure 2A). To measure κ, we first calculate *R*, the radius of curvature at each point along the centerline (κ = 1/*R*). To compare data from different animals, we measure distance along the worm body as the fractional distance from head to tail (head = 0; tail = 1), and normalize curvature using *L*, the total length of the body centerline (normalized curvature = κ × *L*). During sustained forward movement, each body region alternates between positive and negative curvature, and bands of curvature propagate from head to tail as shown in a kymogram (red, positive; blue, negative) (Figures 2B and 2C). Curvatures measured near the head tend to be larger than curvatures measured near the tail (Figure 2D).

First, we asked how the motor activity in one body region might be affected by the bending of neighboring body regions. To do this, we designed microfluidic devices that immobilized body regions of varying length (Figures 3A and 3B; Movie S1 available online). Our first device trapped the center of a worm in a narrow straight channel to keep it from bending without impeding worm movement either anterior or posterior to the channel (Figures 3A and 3B). We used a channel diameter (40 μm) that was sufficient to immobilize the trapped region of a young adult worm (worm diameter is 54 ± 4 μm; mean ± SD) with minimum constriction.

We consistently recorded bouts of forward movement (>10 s) when we immobilized a middle portion of the worm (Figures 3A–3C). Bending waves would propagate normally to the anterior limit of the channel (orange data points in Figure 3D). Short channels (100 μm long) did not affect wave propagation to the tail; the bending wave that emerged from the posterior limit of the channel (black data points in Figure 3D) exhibited similar amplitude as a freely swimming worm (Figure 2D). However, increasing channel length beyond 200 μm significantly diminished the bending amplitude in the posterior body region (Figure 3D). Increasing channel length also augmented the bending amplitude of the anterior body region, perhaps reflecting an increased effort to escape the channel. Fixing the channel length, but moving it toward the tail, also reduced the posterior bending amplitude (Figure 3E).

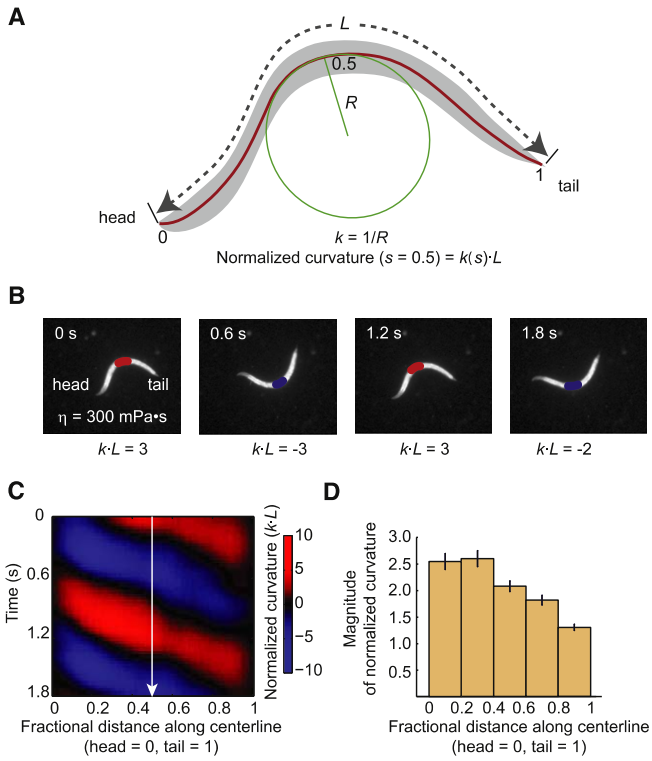

Figure 2. Quantification of Undulatory Dynamics

(A) Worm undulatory dynamics is quantified using time-varying curvature along the body. Points along the centerline of length *L* can be specified in terms of fractional distance from the head (head = 0; tail = 1). The radius of curvature *R* can be measured at all points along the body. Curvature, κ, is the reciprocal of *R*. To represent bending in nondimensional units, we calculate a normalized curvature as κ multiplied by worm length *L*.

(B) Video images of a worm swimming forward. A red-blue colormap illustrates alternating curvatures at fractional distance = 0.5.

(C) Kymogram of time-varying curvature illustrating retrograde bending waves along the worm represented in nondimensional units.

(D) Bending magnitude along the body of a wild-type freely swimming worm, measured as the standard deviation of normalized curvature over time. n = 18 worms, mean ± SEM.

To determine how immobilization affects muscle activity within and posterior to the channel, we quantified intracellular calcium dynamics in the muscle cells of transgenic animals coexpressing the calcium indicator GCaMP3 (Tian et al., 2009) and RFP in all body wall muscles (Figure S1; Movie S2). In these animals, intracellular calcium levels can be inferred from the ratio of green to red fluorescence. Whereas muscle cells anterior to the channel exhibited strong rhythmic calcium dynamics during the propagation of bending waves, muscle cells within and posterior to the channel did not (Figure S1). Thus, immobilizing a body region disrupts the propagation of bending waves by lowering motor circuit activity within and posterior to that region. The tail was held rigid and straight in the absence of muscle activity because of the high internal hydrostatic pressure of worms.

Taken together, these results suggest that immobilizing a portion of the worm can directly override rhythmic activity. Motor activity in a posterior region requires the active bending of an anterior region extending ~200 μm.

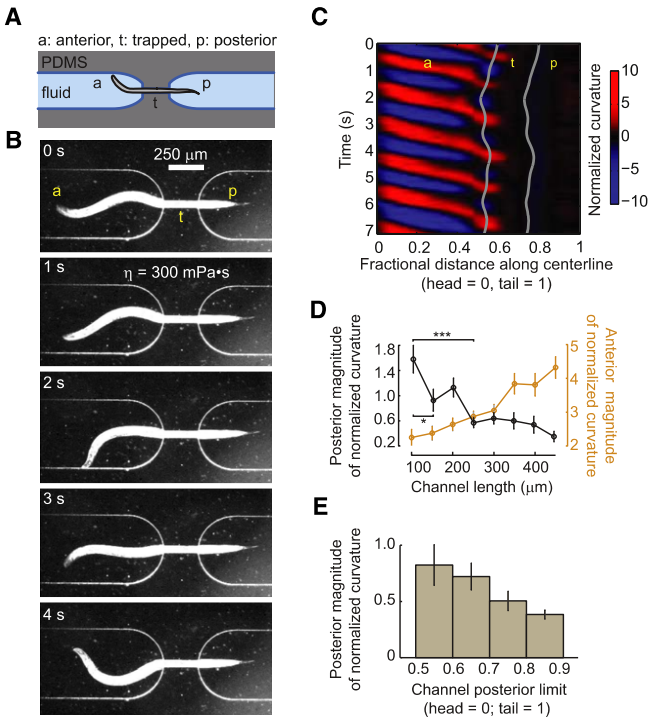

Figure 3. Bending of Posterior Regions Requires Anterior Bending

(A) Schematic of microfluidic device. *a* stands for anterior region, *p* stands for posterior region, and *t* stands for trapped region of a worm. PDMS: Polydimethylsiloxane.

(B) Video images of a wild-type young adult worm exhibiting forward undulatory gait inside the microfluidic device (see also Movie S1). The channel divides the worm body into unrestrained anterior, posterior, and trapped middle regions.

(C) Kymogram of time-varying curvature along the body of the worm shown in (B). Gray lines mark the anterior and posterior limits of the straight channel.

(D) Bending magnitude of a posterior and an anterior body region (~0.15 worm length) adjacent to the channel, measured as the standard deviation of time-varying normalized curvature, is plotted as a function of the length of the trapped region. $n \geq 10$ worms for each condition, mean ± SEM. Position of the posterior limit of the channel is 0.7 ± 0.1 (mean ± standard deviation) for each condition, measured as the fractional distance from head to tail. *$p < 0.05$, ***$p < 0.001$, Mann-Whitney U test.

(E) Bending magnitude of a posterior body region (mean ± SEM) decreases with the position of the posterior limit of the channel ($R = -0.24$, $p < 0.05$, Spearman's rank correlation test). We measured 64 bouts of forward movement trapped in different channel positions from 20 worms. Channel length is 300 μm.

See also Figure S1.

Muscle Activity Is Positively Correlated with the Curvature of Adjacent Anterior Neighbors

To further explore how the bending of adjacent body regions is coupled, we designed microfluidic devices that trapped the middle region of a worm at defined curvatures (Figures 4A and 4C). We used channels that were at least 250 μm long to prevent bending waves from propagating into the unrestrained posterior part. We found that the unrestrained posterior region exhibited fixed curvature in the same direction as that imposed on the middle trapped region (e.g., compare the overall shape of the posterior region to the trapped region in Figure 4A and the measured curvature of the posterior region to the trapped region in the kymogram in Figure 4B; also see Movie S3). By using channels with different curvatures, we found that the curvature of the posterior region increased linearly with the imposed curvature on the trapped middle region with slope 0.62 ± 0.03 L^{-1} (Figures 4C, S2A, and S2B).

We verified that the fixed curvature of the unrestrained posterior region was due to a fixed pattern of muscle activity. First, by using a transgenic strain that expresses halorhodopsin (Han and Boyden, 2007) in all body wall muscles (P*myo-3*::*NpHR*), we were able to induce muscle relaxation in the posterior region with green light illumination. The tail reversibly straightened during illumination (Figures 4D–4F; Movie S4). Second, we directly monitored muscle activity in the curved posterior region using the muscle calcium reporter GCaMP3 (Figure 4G). In the posterior region emerging from the channel, we consistently measured higher calcium levels in the muscle cells on the inner side than the outer side of the curved body (Figures 4H and 4I; Movie S5). Third, when the whole animal was paralyzed with sodium azide, the body regions emerging from the curved channel remained straight, instead of following the curvature imposed by the channel (Movie S6).

These results suggest that the bending of anterior body regions dictates the bending of posterior body regions during forward movement. Posterior regions bend in the same direction as, and in proportion to, the bend of anterior regions.

Postchannel Body Curvature Follows Channel Curvature with a Viscosity-Dependent Delay

Next, we measured the time lag between the bending in one body region and the induced bending in the posterior region. To do this, we designed pneumatic microfluidic devices to rapidly change the curvature of a trapped worm (Figure 5A). We flanked both sides of the immobilizing channel with independently controllable inflatable chambers. As with static channels, we found that the curvature of the posterior body was positively correlated with channel curvature. Switching channel curvature toward the dorsal or ventral side induced a corresponding switch in the curvature of the posterior body (Figures 5B and 5C; Movie S7). This result underscores dorsal/ventral symmetry in the mechanism that couples the curvature of adjacent body regions.

We found that the switch in curvature of the posterior region propagated with measurable speed from the channel to the tail, consistent with the flow of a retrograde bending signal (Figures 5D–5F). To assess whether the delayed bending of the posterior region represented mechanical damping by the external viscous fluid or internal delays within the neuromuscular network, we studied worms in fluids of different viscosity (Figures 5D–5F). We found that the bending delay was roughly constant, ~300 ms, in fluids ranging from 1 mPa·s (the viscosity of water) to ~100 mPa·s. In more viscous fluids, the bending delay began to increase, becoming ~1 s at 300 mPa·s. These results suggest that ~300 ms represents an upper bound for delays within the neuromuscular network, which are rate-limiting at low viscosities. These neuromuscular delays might reflect delays in synaptic transmission and/or the limiting speed of muscle contraction.

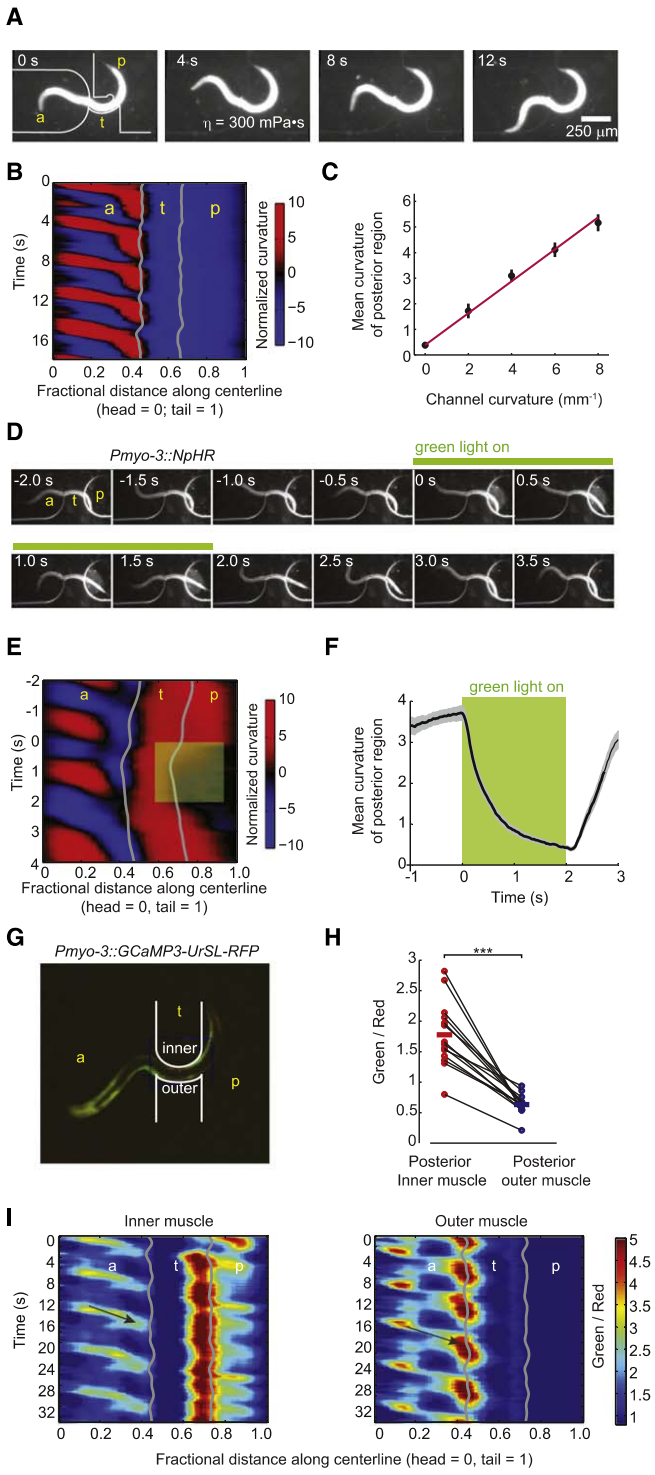

Figure 4. Bending of Posterior Regions Is Positively Correlated with Anterior Bending

(A) Video images of a worm exhibiting forward undulatory gait while partially constrained in a curved microfluidic channel (see also Movie S3; Figure S2).

(B) Kymogram of normalized curvature of the worm shown in (A). Gray lines show anterior and posterior limits of the curved channel. See also Figure S2.

(C) The curvature of the unrestrained posterior body region, measured as a spatial average from the posterior limit of the channel to the tail and a temporal average over bouts of forward movement, is plotted as a function of channel curvature. Each data point (mean ± SEM) represents data from at least eight animals. Magenta line is the linear least square fit. See also Figure S2.

(D) Video images of a transgenic worm (P*myo-3*::*NpHR*) partially constrained in a curved microfluidic channel. The green bar indicates a 2 s interval during which the posterior body wall muscles emerging from the channel was hyperpolarized by green light illumination (see also Movie S4).

(E) Kymogram of normalized curvature of the animal shown in (D). Green shading indicates the body region and duration of green light illumination.

(F) Mean curvature ± SEM of the posterior region emerging from the curved channels as shown in (D) during green light illumination (~30 measurements using six worms).

(G) Calcium imaging of body wall muscles in a partially constrained transgenic worm (P*myo-3*::*GCaMP3*::*RFP*) in a curved channel. Red fluorescence from RFP constitutes the reference signal. Green fluorescence from GCaMP3 indicates intracellular calcium levels. The contours of the microfluidic channel are drawn in white (see also Movie S5).

(H) Comparison of the ratio of green fluorescence to red fluorescence intensity emitted from inner and outer muscles of the posterior body region. Each data point represents a spatial average of the ratio over a posterior body region (~0.2 worm length) adjacent to the channel and a temporal average over a bout of forward movement. Solid lines indicate population mean. Among 14 measurements from six worms, six measurements restrict dorsal muscles on the inner side. ***$p < 0.001$, Wilcoxon signed rank test.

(I) Representative ratiometric kymogram of calcium levels in inner and outer muscle cells of a worm trapped in the device shown in (G). Higher/lower ratios of green fluorescence to red fluorescence in each set of body wall muscles indicate higher/lower intracellular calcium levels. Arrows highlight one calcium wave that propagates from the head to the anterior limit of the curved channel along the inner musculature and outer musculature.

See also Movie S5.

Local Proprioceptive Coupling Is Transduced by B-type Motor Neurons

The *C. elegans* wiring diagram offers a small number of candidate cell types within the motor circuit that might play roles in generating or propagating a local proprioceptive signal: the A-type cholinergic motor neurons, B-type cholinergic motor neurons, the D-type GABAergic motor neurons, and muscle cells. One neuron outside the core motor circuit, the DVA interneuron, has also been shown to exhibit proprioceptive properties (Li et al., 2006). We sought to determine which cell type was responsible for coupling the bending activities of adjacent body regions through proprioception.

First, we trapped transgenic worms that expressed halorhodopsin in all cholinergic motor neurons (P*unc-17*::*NpHR*) in the pneumatic devices and illuminated them with green light. We found that light-induced hyperpolarization of the cholinergic neurons prevented the posterior body regions from following induced changes in the curvature of the anterior region (Figures 6A–6C and Movie S8). Instead, optogenetic inactivation of the cholinergic neurons locked the posterior region in the posture as it was immediately preceding illumination.

Second, we studied *vab-7* mutants, which have specific defects in the morphology of the dorsal B-type cholinergic motor neurons. In these mutants, the DB neurons reverse the orientation of their axons so that they project anteriorly instead of posteriorly (Esmaeili et al., 2002) (Figure S3A) The *vab-7* mutation does not affect the ventral B-type motor neurons. During unrestrained forward movement, the bending wave near the head of *vab-7* mutants was normal. However, the bending wave that

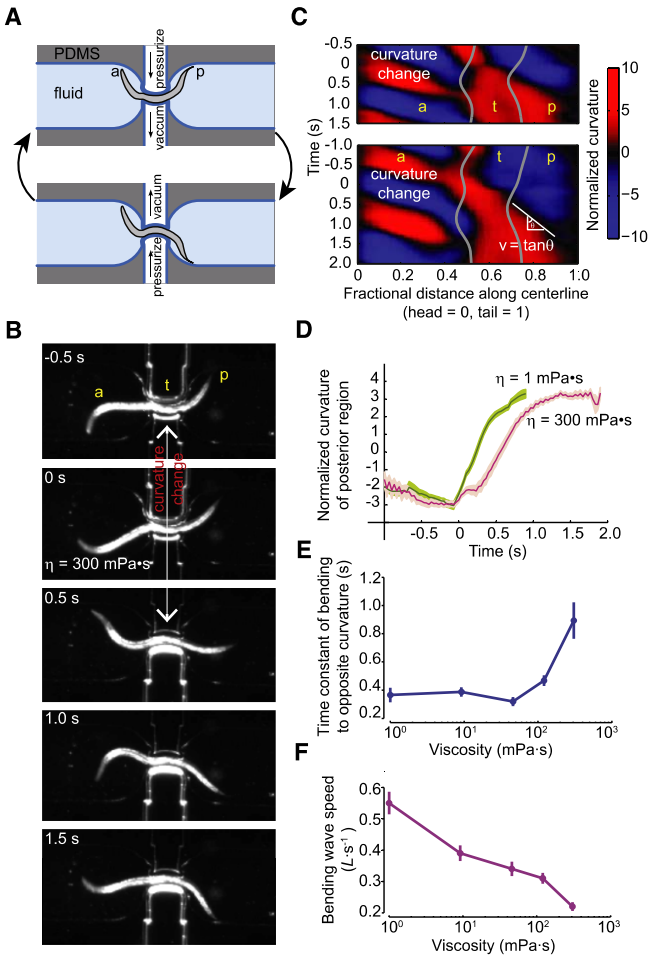

Figure 5. Pneumatic Microfluidic Device for Manipulating Body Curvature

(A) Schematic of the pneumatic microfluidic device. The channel is flanked by two chambers. Alternately pressurizing one chamber while depressurizing the other rapidly switches the curvature the curvature of a region of a trapped worm.

(B) Video images of a partially immobilized wild-type worm. At t = 0 s, the channel starts to change its curvature (see also Movie S7).

(C) Two representative curvature kymograms of a worm trapped in the pneumatic channel. Gray lines mark the anterior and posterior limits of the curved channels. White dashed lines at t = 0 s mark the induced change in channel curvature from negative (color blue) to positive (color red). While the unrestricted anterior body region exhibits opposite bending activities in the two kymograms, this difference did not affect the dynamics of the induced curvature change in the unrestricted posterior body region. The bending wave that shifts the posterior region from negative to positive curvature propagates with a velocity v that is the reciprocal slope of the zero crossing in curvature (color black). A white line is drawn along the zero crossing, and velocity is calculated from its angle with respect to the vertical axis, $v = \tan\theta$.

(D) The time course of curvature change in the immediate posterior region (~0.1 worm length) emerging from the pneumatic channel after the switch of channel curvature at t = 0 s. The two curves correspond to experiments conducted in two different viscosities. Error bars indicate SEM.

(E) The time constant for relaxation of the posterior region to new curvatures obtained by fitting exponentials to time courses as shown in (D). Each data point represents at least 30 measurements from five worms. Error bars indicate 95% confidence interval to the exponential fits.

(F) The speed of the bending wave following induced changes in channel curvature as a function of fluid viscosity. Error bars indicate SEM.

propagates to posterior regions was biased toward the ventral side (Figures S3B and S3D). When we trapped *vab-7* mutants in the pneumatic channels, the posterior region was only able to follow channel bending to the ventral side, not to the dorsal side (Figures S3C, S3F, and S3G). These results suggest that the dorsal and ventral B-type cholinergic motor neurons are each responsible for propagating dorsal and ventral curvatures to posterior body regions.

Third, we compared the effects of specifically inactivating the A-, B-, and D-type motor neurons. To do this, we examined transgenic animals in which either the A- or B-type cholinergic motor neurons are specifically deactivated by an active K^+ channel (P*unc-4*::*twk-18*(gf)-*UrSL-wCherry* and P*acr-5*::*twk-18*(gf)-*UrSL-wCherry*, respectively) (Kawano et al., 2011; Kunkel et al., 2000), as well as *unc-25* mutants that lack the GABA neurotransmitter required by the D-type motor neurons (Jin et al., 1999). During forward locomotion, the bending waves of animals propagated from head to tail when either the A-or D-type motor neurons were inactivated (Figures S4A and S4C). When trapping the worm in the pneumatic microfluidic device, the posterior region of these worms followed the induced body bending toward either side (Figures S4B and S4D). In contrast, inactivating the B-type motor neurons prevented an induced bend from anterior regions from propagating to posterior regions (Figures 6D–6F; Movie S9). When the B-type motor neurons were inactivated, the curvature of the posterior region was not locked to the curvature of the trapped region (Figures 6D and 6E) as for wild-type worms (Figures 4A and 4B).

The *C. elegans* motor circuit does not possess local sensory or interneurons that convey local bending information to B-type motor neurons. The DVA interneuron, whose axon spans the whole worm body and connects with most DB motor neurons, has been shown to have proprioceptive properties (Hu et al., 2011; Li et al., 2006). We thus asked whether DVA plays a role in propagating local bending information during forward locomotion. However, we found that laser killing DVA does not disrupt the ability of the posterior region to follow the curvature of the anterior region (Figures S4G and S4H). Taken together, these results show that neither the A- and D-type motor neurons nor the DVA interneuron are needed to propagate the bending signal from anterior to posterior regions. However, the B-type motor neurons are essential.

Gap Junctions between Muscle Cells Do Not Contribute to Proprioceptive Coupling

We also asked whether the body muscle cells themselves might propagate bending signals from anterior to posterior regions. Adjacent body wall muscle cells are connected by gap junctions mediated specifically by an innexin UNC-9, providing a possible alternative pathway for transducing the proprioceptive signal (Figure 1B) (Liu et al., 2006). First, we trapped transgenic worms expressing halorhodopsin in their muscle cells (P*myo-3*::*NpHR*) in the pneumatic channel. We found that specifically relaxing the muscles in the trapped curved region with green light illumination had no effect on the curvature of the free posterior region (Figures S4E and S4F). We also tested transgenic animals that lacked these gap junctions in their muscle cells. To do this, we used a transgenic *unc-9* mutant animal in which *unc-9*

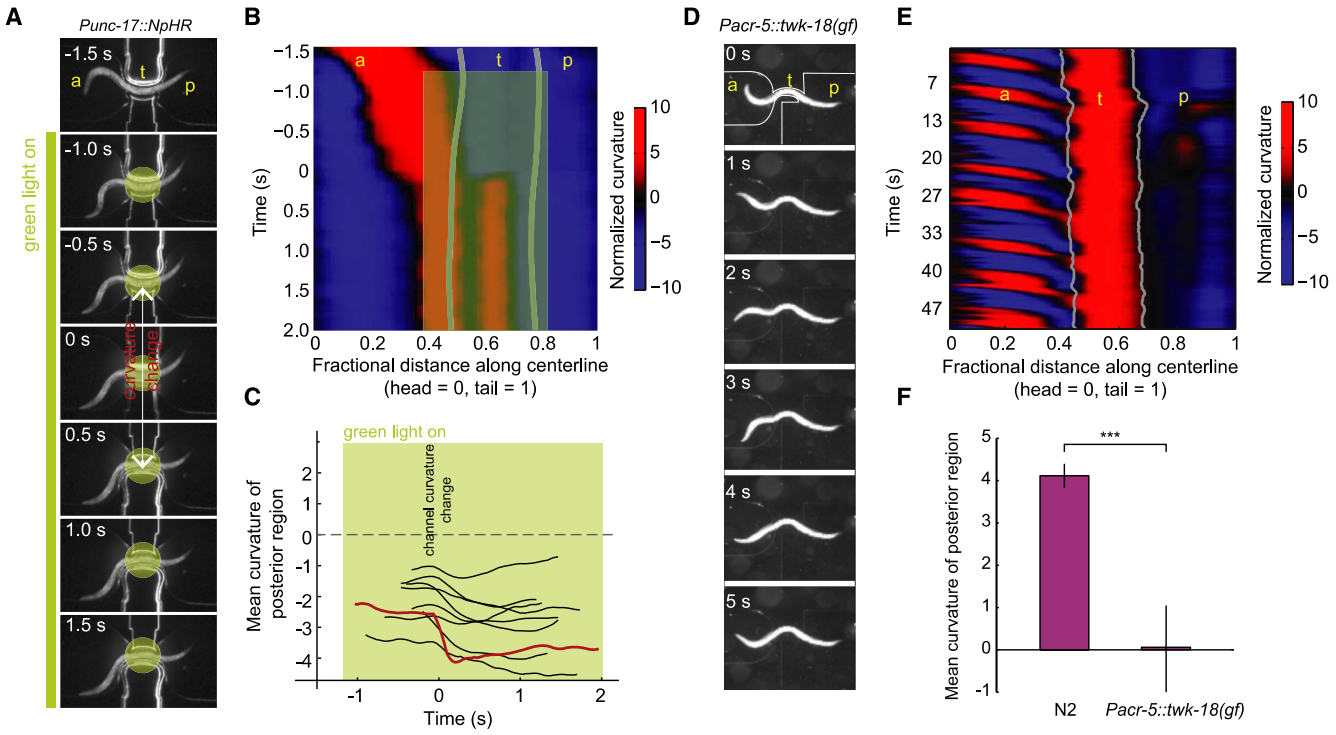

Figure 6. B-type Cholinergic Motor Neurons Are Required for Transducing the Proprioceptive Signal

(A) Video images of a transgenic worm (P*unc-17::NpHR*) partially trapped in a pneumatic microfluidic channel. Green bar indicates the duration of green light illumination of the middle portion of the worm before and after induced change in channel curvature at $t = 0$ s. As a result, the curvature of the tail failed to follow the curvature change of the channel. See also Movie S8.

(B) Curvature kymogram of the transgenic worm trapped in the channel as shown in (A). Green shading indicates the body region and duration of green light illumination. See also Movie S8.

(C) Curvature of the posterior body region, measured as an average from the posterior limit of the channel to the tail, during onset of illumination (green shading) and the induced change in curvature of the middle region at $t = 0$ (dashed line). Representative data from five worms were shown. Red curve corresponds to the experiment shown in (A) and (B). A comparison with Figure 5D shows that posterior body region did not switch its curvature after induced curvature change in the trapped middle region during green light illumination. See also Movie S8.

(D) Video images of a P*acr*-5::*twk-18*(gf)-*UrSL-wCherry* transgenic worm partially trapped in a static microfluidic channel. B-type cholinergic motor neurons in this strain were specifically deactivated because of the expression of an active K^+ channel. See also Movie S9.

(E) Curvature kymogram of the partially trapped worm shown in (D) during periods of forward movement. A comparison with Figures 3B shows that the posterior body region emerged from the channel no longer follow the curvature of the middle region imposed by the channel. See also Movie S9.

(F) The mean curvature of the posterior body region emerged from the microfluidic channel in wild-type (n = 8) and P*acr*-5::*twk*-18(gf)-*UrSL-wCherry* transgenic worms (n = 9) during forward movement. All worms were partially trapped in the channel with a curvature 6–8 mm^{-1}. Error bars are S.E.M. ***$p < 0.001$, Mann-Whitney U test. See also Movie S9.

See also Figures S3, S4, and S5.

expression was restored in UNC-9-expressing cells except the body wall muscles. We found that these transgenic animals were fully capable of propagating an imposed bend from anterior to posterior regions (Figure S4H).

As a further test of gap junctions between muscle cells, we optogenetically stimulated body segments in transgenic worms expressing Channelrhodopsin-2 in body wall muscles (P*myo*-3::*ChR2*) without input from motor neurons. To abolish motor neuron inputs, we treated transgenic worms with ivermectin, which hyperpolarizes the motor circuit by activating glutamate gated chloride channel (Cully et al., 1994) but is not known to affect body wall muscles (Hart, 2006). Optogenetically inducing ventral or dorsal bending in targeted body segments of paralyzed animals did not induce bending of neighboring regions (n > 10; Figures S5A and S5B; Movie S10). We observed similar phenomenon when ivermectin treatment was performed in the *unc-13(s69)* (n > 10), a loss of function mutation that eliminates synaptic input from motor neurons to muscles (Richmond et al., 1999). These experiments suggest that gap junctions between muscles are insufficient to propagate bending signals between neighboring body regions.

Interestingly, when we optogenetically induced body bending in ivermectin-treated paralyzed worms, the bend would persist long after turning off the illumination (Figures S5A and S5B; Movie S10). The bend would gradually relax over ~40 s, but often in a series of abrupt jumps (Figure S5C). This observation suggests that body wall muscles can exhibit hysteresis: maintaining stable levels of contraction long after stimulation. This observation could also explain why inactivating cholinergic motor neurons in transgenic worms (P*unc-17::NpHR*) locks

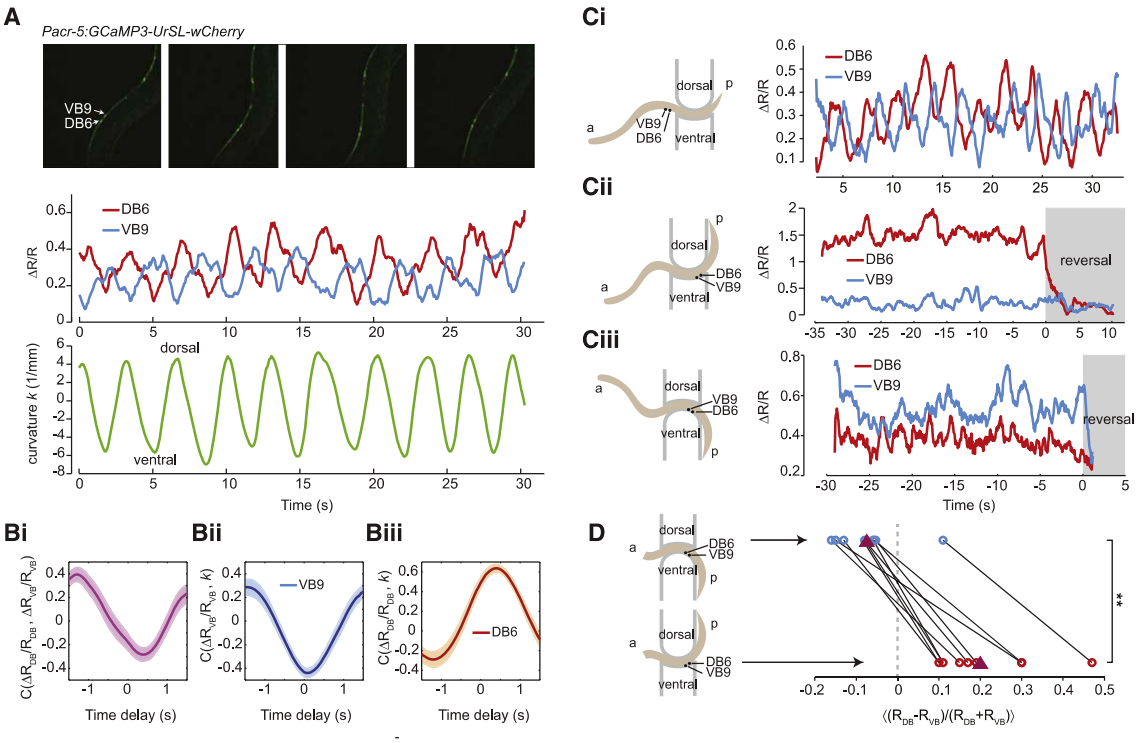

Figure 7. Calcium Imaging of B-type Motor Neuron Activity Induced by Bend-Sensitive Coupling

(A) Calcium imaging of B motor neuron activity in a forward moving worm. Worms are slightly compressed in the lateral direction (left and right) so that the body movement is confined within a focal plane to allow simultaneous multi-neuron recording. Upper panel: fluorescent video images of two adjacent motor neurons VB9 and DB6 in an unrestrained transgenic worm (P*acr-5*::*GCaMP3-UrSL-wCherry*) swimming within a microfluidic chamber. Middle panel: intracellular calcium dynamics of VB9 and DB6. Lower panel: curvature of the corresponding body region. The intracellular calcium activity can be inferred from the ratio of *GCaMP3* fluorescence intensity to *wCherry* fluorescence intensity. Red fluorescence from wCherry constitutes the reference signal. $\Delta R/R$ is the relative deviation of the emission ratio from the baseline.

(B) Cross-correlation between VB9 and DB6 calcium dynamics of forward moving worms (Bi). Cross-correlation between VB9 calcium dynamics and the curvature of corresponding body region (Bii). Cross-correlation between DB6 calcium dynamics and the curvature of corresponding body region (Biii). n = 9 and error bars indicate SEM.

(C) Representative intracellular calcium dynamics of motor neurons DB6 and VB9 located anterior to the channel. During forward movement, these two neurons exhibited anticorrelated oscillatory calcium activities (Ci). Intracellular calcium dynamics of VB9 and DB6 when the body region containing both neurons was imposed to bend toward the dorsal side (Cii). DB6 sustained a higher level of calcium activity (Cii). Calcium dynamics of VB9 and DB6 when the body region containing both neurons was imposed to bend toward the ventral side (Ciii). VB9 sustained a higher level of calcium activity. In both cases, the calcium dynamics in VB9 and DB6 inactivated during reversal (Ciii).

(D) Difference of intracellular calcium activity between DB6 and VB9 when the body region containing both neurons were imposed to bend either toward dorsal or ventral side. This quantity is normalized by the total calcium activity of DB6 and VB9 and averaged over a time period (>20 s) when a worm was moving forward. Each black line represents a different worm and magenta triangles represent the population mean. **p < 0.005, Wilcoxon signed rank test. n = 10 worms.

them in the posture immediately preceding illumination (Figures 6A–6C; Leifer et al., 2011).

Bending Directly Activates B-type Motor Neurons

Our results thus suggest that the B-type cholinergic motor neurons represent the locus for proprioceptive coupling during forward movement. Next, we sought direct physiological evidence for the proprioceptive properties of the B-type motor neurons. First, we measured the intracellular calcium dynamics of individual DB and VB neurons of unrestrained worms swimming inside microfluidic chambers (P*acr-5-GCaMP3-UrSL-wCherry*). Consistent with an earlier study (Kawano et al., 2011), the calcium dynamics of DB6 and VB9, two motor neurons that innervate the opposing dorsal and ventral body wall muscles, respectively, are negatively correlated with one another during forward movement (Figure 7A). The cross-correlation between the time-varying calcium signals from DB6 and VB9 are presented in Figure 7Bi. Furthermore, we measured the cross-correlation between motor neuron activity and the local curvature of the worm at the position of the cell bodies of the motor neurons. We found that the activity of the ventral motor neuron (VB9) is positively correlated with bending toward the ventral side (Figure 7Bii), and the activity of the dorsal cholinergic neuron (DB6) is positively correlated with bending toward the dorsal side (Figure 7Biii). These results confirm that the sign and amount of local bending is strongly coupled to the activity level in the B-type motor neurons.

To determine whether the bending of anterior regions directly determines the activity of posterior B-type motor neurons, we

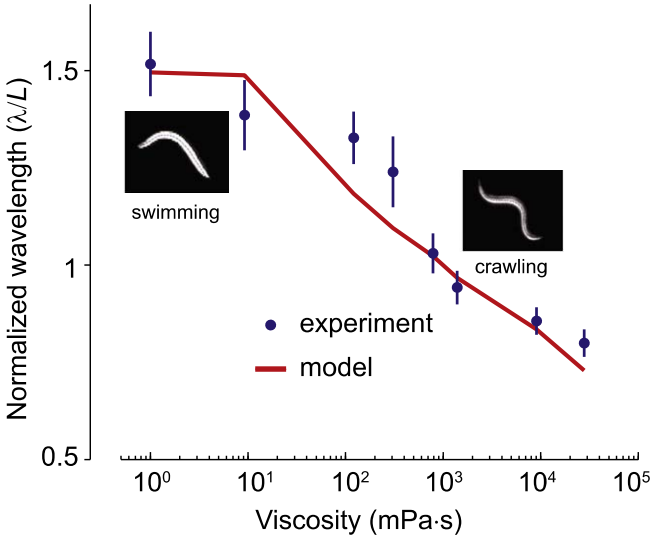

Figure 8. The Dynamics of Proprioception within the Motor Circuit Are Consistent with Continuous Gait Adaptation

Theoretically predicted dependence of undulation wavelength on external viscosity (red; also see Equation 1) closely fit the experimental measurements (blue). Error bars are 95% confidence interval.

visualized their calcium dynamics using our curved microfluidic channels. When we imposed a curvature on the middle portion of a worm, bending waves propagated normally from the head to the anterior limit of the channel. When we positioned specific DB and VB motor neurons near the anterior limit of the channel, we observed rhythmic activity correlated with dorsal and ventral bending, respectively (Figure 7Ci). When we positioned the same DB and VB motor neurons within or near the posterior limit of the channel, we observed fixed patterns of activity that reflected the curvature imposed by the channel. Bending the worm toward the dorsal side activated the DB motor neuron over the VB motor neuron (Figures 7Cii and 7D). Bending the worm toward the ventral side activated the VB motor neuron over the DB motor neuron (Figures 7Ciii and 7D). These fixed patterns of B-type motor neuron activities relaxed when the worm spontaneously transitioned to backward movement (Figures 7Cii and 7Ciii).

Proprioception Is Consistent with Gait Adaptation in Response to Mechanical Load

Unlike larger well-studied swimmers such as the leech and lamprey, *C. elegans* is smaller than the capillary length of water (~2 mm). At this size, forces due to surface tension that hold the crawling animal to substrates are 10,000-fold larger than forces due to the viscosity of water (Sauvage, 2007). Thus, the motor circuit of *C. elegans* must adapt to extreme ranges of external load. When worms swim in low-load environments such as water, the bending wave has a long wavelength (~1.5 body length *L*). When crawling or swimming in high-load environments ~10,000-fold more viscous than water, the bending wave has a short wavelength (~0.65 *L*). We asked whether the spatiotemporal dynamics of proprioceptive coupling between body regions plays a role in this gait adaptation.

In our model, we assert that the undulatory wave begins with rhythmic dorsal/ventral bends near the head of a worm. Along the body, however, we assert only the dynamics of proprioceptive coupling measured here and previously measured biomechanics of the worm body. We model the muscles in each body region as being directly activated by bending detected in the neighboring anterior region. We can infer the spatial extent of this coupling *l* to be ~200 μm based on our direct measurements (Figure 3D). For a 1-mm-long worm freely swimming in water, the maximum speed of undulatory wave propagation from head to tail is ~2.6 mm/s. Thus, we can estimate the limiting delay τ_c for transducing a bending signal from region to region to be 75 ms. The simplest linear model for motor circuit activity along the body is fully defined in terms of these parameters, along with biomechanical parameters that were measured in previous work (Fang-Yen et al., 2010): the mechanical drag imposed by the environment and the bending modulus of the worm *b*. This model can be solved analytically for the wavelength of bending waves, λ:

$$\lambda = \frac{2\pi l}{\omega C_N (\lambda/2\pi)^4 / b + \omega\tau_c}. \qquad \text{(Equation 1)}$$

Here, $C_N \approx 30\eta$ is the frictional drag coefficient normal to the body centerline, where η is the fluid viscosity, $b = 9.5 \times 10^{-14}$ Nm^2, and ω is the angular frequency of undulation in fluid with different viscosities (Fang-Yen et al., 2010). Equation 1 predicts a specific dependence of bending wavelength on fluid viscosity that closely fits experimental observations (Figure 8; Supplemental Information).

Proprioception within the motor circuit provides a simple explanation for the propagation of bending waves along the motor circuit. Each body region is compelled to bend shortly after the bending of anterior regions, so that the rhythmic bending activity initiated near the head can generate a wave of rhythmic activity that travels along the whole body. When viewed within the biomechanical framework of the worm body, the spatiotemporal dynamics of proprioception within the motor circuit provides an explanation for the adaptation of undulatory gait on mechanical load.

DISCUSSION

Prevailing models for rhythmic movements in larger animals involve networks of CPGs that are modulated and entrained by sensory feedback (Marder and Bucher, 2001). For example, the lamprey spinal cord consists of approximately 100 independent CPG units distributed along its length (Cangiano and Grillner, 2003). In most systems, coherent rhythmic movements across the whole body are organized by proprioceptive and mechanosensory feedback to CPG units (McClellan and Jang, 1993; Pearson, 1995; Yu and Friesen, 2004). In the leech, muscle activity between body segments can be coordinated by sensory feedback even after severing the neuronal connectivity between segments (Yu et al., 1999). In *Drosophila* larvae, specific classes of mechanosensory neurons are required to propagate peristaltic waves during locomotion (Cheng et al., 2010; Hughes and Thomas, 2007; Song et al., 2007).

Here, we found a previously undescribed role for proprioception within the motor circuit for propagating rhythmic activities along the body. We show that, during forward locomotion, bending waves are driven along the body through a chain of reflexes connecting the activity of neighboring body segments. Unlike larger animals, *C. elegans* does not have dedicated local sensory or interneurons that might generate or propagate proprioceptive signals within the motor circuit. The cellular economy of the *C. elegans* wiring diagram implies that individual neurons may have high levels of complexity. Indeed, we have found that the proprioceptive feedback loop that drives forward locomotion is transduced within motor neurons themselves, specifically the B-type cholinergic neurons. The activity of each VB and DB motor neuron is directly activated by ventral and dorsal bending of an anterior region, respectively. Axons of adjacent B-type cholinergic neurons are not anatomically restricted to specific segments, but partially overlap with one another in the ventral and dorsal nerve cords. Thus, going from head to tail, a large posterior portion of each B-type cholinergic neuron runs parallel to the anterior portion of its neighbor in the ventral and dorsal nerve cords. These overlapping portions, along with gap junctions between adjacent neurons, may provide an anatomic platform for propagating a bending signal from neuron to neuron (Figure S6). In *vab-7* mutants, the reversed axon projection of DB motor neurons prevents the dorsal posterior bending wave propagation. Disruption of the wiring pattern on the dorsal side, but not the ventral side, of *vab-7* mutants might thus explain the specific disruption of dorsal bending waves to the tail.

Both DB and VB motor neurons also have long undifferentiated processes that extend posteriorly beyond their regions of synaptic output to the muscle cells (Figures 1C and S6). We note that this anatomical property of the B-type motor neurons led Russell and Byerly to propose that these processes might have proprioceptive properties. If proprioception were specifically localized to these processes, they would communicate bending signals from posterior to anterior. Because the B-type neurons propagate signals from anterior to posterior, as we have found, the long posterior projections of the B-type motor neurons are unlikely to represent the specialized "proprioceptive antennae," and we would expect the relevant mechanosensitive elements to be localized near their anterior processes.

One candidate for a potential mechanosensitive channel expressed in the cholinergic motor neurons is the *unc-8* gene that encodes a putative mechanically gated ion channel. However, an *unc-8(lf)* mutation did not disrupt proprioceptive coupling between neighboring body regions (Figure S4H), and the mutant moves like wild-type animals. Thus, the molecular mechanism that confers proprioceptive properties to the B-type motor neurons remains to be identified. Identifying genetic lesions that disrupt proprioception in the B-type cholinergic motor neurons would help define the molecular mechanisms. Disruption of these mechanosensitive elements would specifically abolish the propagation of bending waves.

Unlike systems such as the leech, lamprey, or vertebrate spinal cord, *C. elegans* does not appear to depend on a distribution of CPGs along its motor circuit to propagate bending waves. In *C. elegans*, proprioceptive information is used to directly drive the bending of posterior segments based on the bending of anterior segments, not to entrain the rhythms of separate CPG elements. We propose that a CPG operates near the head of the worm to generate the rhythmic bending of the most anterior segment. Proprioception within the motor circuit, however, suffices to translate the rhythmic activity near the head to sustained undulatory waves along the body.

This form of sensory feedback makes the motor circuit directly responsive to the external environment. We used our biophysical measurements to calculate the effect of proprioception on undulatory waves in surroundings with different viscosities and uncovered a compelling explanation for the adaptation of undulatory wavelength on external load. At low loads, the worm undulates with a long wavelength. At high loads, the worm undulates with a short wavelength. This dependence has an intuitive biomechanical explanation. As external viscosity increases, it takes longer for a posterior body region to bend in response to any curvature change in its anterior neighbor. Increasing the time scale of the bending response increases the phase difference between the shapes of neighboring body segments, leading to a smaller undulation wavelength.

The small size and experimental accessibility of the *C. elegans* motor circuit allows the possibility of modeling locomotion that integrates the dynamics of all neuronal and muscular components. Our results suggest that a full model of *C. elegans* locomotion must integrate the biomechanics of undulatory movement with neuromuscular activity to properly incorporate the role of proprioception within the motor circuit.

EXPERIMENTAL PROCEDURES

Worm Strains and Cultivation

Wild-type, transgenic, and mutant worms were cultivated using standard methods (Brenner, 1974). Detailed strain information can be found in the Supplemental Information. The transgenic worms used in all optogenetic experiments were cultivated in the dark at 20°C on NGM plates with *Escherichia coli* OP50 and all-*trans* retinal. We performed all experiments using adult hermaphrodites within a few hours after their final molt.

Microfluidic Devices

Custom microfluidic devices were fabricated in PDMS using soft lithography techniques. In the pneumatic microfluidic device, the channel was flanked by two chambers that could be alternatively pressurized and depressurized with a valve system under computer control using custom software written in LabVIEW (National Instruments, Austin, TX). We loaded each microfluidic channel with NGM buffer or dextran solution (~20% dextran in NGM [wt/vol] in most cases). An individual worm was flowed into the inlet of each microfluidic channel and worm position within each channel was manually controlled by syringes connected to polyethylene tubing.

Measuring Undulatory Dynamics

Experiments were performed on Nikon microscopes (TE2000 or Eclipse LV150) under 4× magnification with dark-field illumination. Image sequences were taken by a CCD camera (Imaging Source) and recorded on a computer at 30 Hz using IC Capture software (Imaging Source). Image analysis was performed using custom software written in MATLAB (MathWorks, Inc. Natick, MA) following methods described in (Fang-Yen et al., 2010).

Calcium Imaging of Body Wall Muscle Activities

We imaged calcium dynamics within muscle cells of worms partially trapped in microfluidic channels, using methods similar to those described in (Chen,

2007). GCaMP3 and RFP were excited by LEDs filtered at 448–492 nm and 554–572 nm, respectively, using Semrock single-bandpass filters. Fluorescence emission was recorded through an Olympus MVX Plan Apochromat 2X objective (working distance, 20 mm; numerical aperture, 0.5). The fluorescence image was split by a Cairns Optosplit II Image Splitter, and the two images (green channel, 499–525 nm; red channel, 581–619 nm) were projected onto two halves of an Andor iXon 885 EMCCD camera. A DinoLite Pro AM413T USB camera was used to track the worm using Worm Tracker 2.0 software developed by the Schafer laboratory. Zaber T-LSR075A Motorized Linear Slides give automated x-y stage movement. Imaging sequences were recorded on a computer at 10 Hz using Andor Solis software and were converted into TIFF files using ImageJ. Images were then analyzed using custom-written MATLAB scripts. Briefly, the two split images were realigned, and the calcium activities of muscles were calculated as the ratio of green to red fluorescence emission intensities. The true emission intensities from the two channels are calculated using the following formulas: True green = green measured − green background; True red = red measured − red background − 0.153 × True green. There is 15.3% bleedthrough from the green to the red channel.

Calcium Imaging of B-type Motor Neurons

We imaged calcium dynamics in B-type cholinergic motor neurons of worms moving in the microfluidic device using a spinning-disk confocal microscopy (Yokogawa). GCaMP3 and wCherry, which are coexpressed in the B-type motor neurons, were excited by a 488 nm blue laser and a 561 nm yellow laser (Andor Technology) alternatively at every 30 ms. Fluorescence emission was collected through a Nikon Plan Apo 20× objective (working distance, 1 mm; numerical aperture, 0.75) and projected onto an Andor iXon2 EMCCD camera. Imaging sequences were recorded using the NIS-elements software and converted into TIFF files. Images were then analyzed using custom-written MATLAB scripts. The motor neurons of interest were automatically identified, and the calcium dynamics in the cells were calculated as the ratio of GCaMP3 to wCherry fluorescence emission intensities from two sequential images using the following formula:

$$R = \frac{I_b - \varepsilon_r I_y}{I_y - \varepsilon_g I_b} \frac{1+\varepsilon_g}{1+\varepsilon_r}, \qquad \text{(Equation 2)}$$

where I_b is total fluorescence emission intensity excited by the blue laser and I_y is the total fluorescence emission intensity excited by the yellow laser. ε_r is the ratio of mCherry emission intensity excited by the blue laser to that excited by the yellow laser. ε_g is the ratio of GCaMP3 emission intensity excited by the yellow laser to that excited by the blue laser. $\varepsilon_r = 0.0356$ and $\varepsilon_g \approx 0$ when the same blue and yellow laser power was used. These ratios were measured using strains expressing only wCherry or GCaMP3 in given neurons.

To measure the correlation between intracellular calcium dynamics in the B-type motor neurons and the bending activity in the corresponding body region, we used canny edge detection method to identify the boundaries of the worm body from the fluorescence images and calculated the curvature of the body segment where the cell body of the motor neurons are located. The cross-correlation between calcium activities and curvature was calculated using the following formula:

$$C_{xy}(\tau) = \frac{\langle \Delta x(t+\tau)\Delta y(t)\rangle}{\sqrt{\langle \Delta x^2(t)\rangle}\sqrt{\langle \Delta y^2(t)\rangle}}, \qquad \text{(Equation 3)}$$

where $\Delta x(t)$ and $\Delta y(t)$ are deviations of x and y from their respective means and $\langle \cdot \rangle$ denotes the average over time.

Optogenetic Stimulation

We used two optical setups to stimulate transgenic worms expressing Channelrhodopsin or Halorhodopsin. Experiments with the pneumatic microfluidic device (Figure 6A) were conducted on a Nikon microscope (Eclipse LV150) under 10× magnification with dark-field illumination. A mercury arc lamp with green filter and field diaphragm was used to illuminate the worm with controlled spot size. Rhodamine in the microfluidic channel (10 μM) allowed us to directly visualize the area and duration of green light illumination. Other optogenetic experiments were performed using a modified version of the CoLBeRT system (Leifer et al., 2011). See Supplemental Information for a more detailed description.

SUPPLEMENTAL INFORMATION

Supplemental Information includes six figures, ten movies, and Supplemental Experimental Procedures and can be found with this article online at http://dx.doi.org/10.1016/j.neuron.2012.08.039.

ACKNOWLEDGMENTS

We are grateful to Christopher Gabel, Cornelia Bargmann, L. Mahadevan, and Yun Zhang for useful discussions; Gal Haspel and Netta Cohen for reading the manuscript; Mason Klein for the help with spinning disk confocal microscopy; and Edward Pym and Zengcai Guo for sharing their strains. This work was supported by NIH Pioneer Award, NSF, and Harvard-MIT Innovation Fund.

Accepted: August 27, 2012
Published: November 21, 2012

REFERENCES

Berri, S., Boyle, J.H., Tassieri, M., Hope, I.A., and Cohen, N. (2009). Forward locomotion of the nematode *C. elegans* is achieved through modulation of a single gait. HFSP J. *3*, 186–193.

Boyle, J.H., Berri, S., and Cohen, N. (2012). Gait modulation in *C. elegans*: An integrated neuromechanical model. Front. Comput. Neurosci. *6*, 10.

Brenner, S. (1974). The genetics of *Caenorhabditis elegans*. Genetics *77*, 71–94.

Brown, T.G. (1911). The intrinsic factors in the act of progression in the mammal. Proc. R. Soc. Lond. B Biol. Sci. *84*, 308–319.

Cang, J., and Friesen, W.O. (2000). Sensory modification of leech swimming: rhythmic activity of ventral stretch receptors can change intersegmental phase relationships. J. Neurosci. *20*, 7822–7829.

Cang, J., Yu, X., and Friesen, W.O. (2001). Sensory modification of leech swimming: interactions between ventral stretch receptors and swim-related neurons. J. Comp. Physiol. A Neuroethol. Sens. Neural Behav. Physiol. *187*, 569–579.

Cangiano, L., and Grillner, S. (2003). Fast and slow locomotor burst generation in the hemispinal cord of the lamprey. J. Neurophysiol. *89*, 2931–2942.

Chalfie, M., Sulston, J.E., White, J.G., Southgate, E., Thomson, J.N., and Brenner, S. (1985). The neural circuit for touch sensitivity in *Caenorhabditis elegans*. J. Neurosci. *5*, 956–964.

Chen, B.L. (2007). Neuronal network of *C. elegans*: from anatomy to behavior. PhD dissertation, The Watson School of Biological Sciences (Cold Spring Harbor, NY: Cold Spring Harbor Laboratory Press), p. 96.

Chen, B.L., Hall, D.H., and Chklovskii, D.B. (2006). Wiring optimization can relate neuronal structure and function. Proc. Natl. Acad. Sci. USA *103*, 4723–4728.

Cheng, L.E., Song, W., Looger, L.L., Jan, L.Y., and Jan, Y.N. (2010). The role of the TRP channel NompC in *Drosophila* larval and adult locomotion. Neuron *67*, 373–380.

Chronis, N., Zimmer, M., and Bargmann, C.I. (2007). Microfluidics for in vivo imaging of neuronal and behavioral activity in *Caenorhabditis elegans*. Nat. Methods *4*, 727–731.

Clark, D.A., Gabel, C.V., Gabel, H., and Samuel, A.D.T. (2007). Temporal activity patterns in thermosensory neurons of freely moving *Caenorhabditis elegans* encode spatial thermal gradients. J. Neurosci. *27*, 6083–6090.

Cohen, A.H., and Wallén, P. (1980). The neuronal correlate of locomotion in fish: "fictive swimming" induced in an in vitro preparation of the lamprey spinal cord. Exp. Brain Res. *41*, 11–18.

Cully, D.F., Vassilatis, D.K., Liu, K.K., Paress, P.S., Van der Ploeg, L.H., Schaeffer, J.M., and Arena, J.P. (1994). Cloning of an avermectin-sensitive glutamate-gated chloride channel from *Caenorhabditis elegans*. Nature *371*, 707–711.

Delcomyn, F. (1980). Neural basis of rhythmic behavior in animals. Science *210*, 492–498.

Durbin, R.M. (1987). Studies on the development and organisation of the nervous system of *Caenorhabditis elegans*. PhD dissertation (Cambridge, UK: University of Cambridge), p. 121.

Esmaeili, B., Ross, J.M., Neades, C., Miller, D.M., 3rd, and Ahringer, J. (2002). The *C. elegans* even-skipped homologue, vab-7, specifies DB motoneurone identity and axon trajectory. Development *129*, 853–862.

Fang-Yen, C., Wyart, M., Xie, J., Kawai, R., Kodger, T., Chen, S., Wen, Q., and Samuel, A.D. (2010). Biomechanical analysis of gait adaptation in the nematode *Caenorhabditis elegans*. Proc. Natl. Acad. Sci. USA *107*, 20323–20328.

Faumont, S., Rondeau, G., Thiele, T.R., Lawton, K.J., McCormick, K.E., Sottile, M., Griesbeck, O., Heckscher, E.S., Roberts, W.M., Doe, C.Q., and Lockery, S.R. (2011). An image-free opto-mechanical system for creating virtual environments and imaging neuronal activity in freely moving *Caenorhabditis elegans*. PLoS ONE *6*, e24666.

Guo, Z.V., Hart, A.C., and Ramanathan, S. (2009). Optical interrogation of neural circuits in *Caenorhabditis elegans*. Nat Methods *6*, 891–896.

Grillner, S. (2003). The motor infrastructure: from ion channels to neuronal networks. Nat. Rev. Neurosci. *4*, 573–586.

Grillner, S., and Wallén, P. (2002). Cellular bases of a vertebrate locomotor system-steering, intersegmental and segmental co-ordination and sensory control. Brain Res. Brain Res. Rev. *40*, 92–106.

Grillner, S., Williams, T., and Lagerbäck, P.A. (1984). The edge cell, a possible intraspinal mechanoreceptor. Science *223*, 500–503.

Han, X., and Boyden, E.S. (2007). Multiple-color optical activation, silencing, and desynchronization of neural activity, with single-spike temporal resolution. PLoS ONE *2*, e299.

Hart, A.C. (2006). Behavior. In: The *C. elegans* Research Community, ed. WormBook. http://www.wormbook.org.

Haspel, G., and O'Donovan, M.J. (2011). A perimotor framework reveals functional segmentation in the motoneuronal network controlling locomotion in *Caenorhabditis elegans*. J. Neurosci. *31*, 14611–14623.

Haspel, G., O'Donovan, M.J., and Hart, A.C. (2010). Motoneurons dedicated to either forward or backward locomotion in the nematode *Caenorhabditis elegans*. J. Neurosci. *30*, 11151–11156.

Hu, Z., Pym, E.C., Babu, K., Vashlishan Murray, A.B., and Kaplan, J.M. (2011). A neuropeptide-mediated stretch response links muscle contraction to changes in neurotransmitter release. Neuron *71*, 92–102.

Hughes, C.L., and Thomas, J.B. (2007). A sensory feedback circuit coordinates muscle activity in *Drosophila*. Mol. Cell. Neurosci. *35*, 383–396.

Jin, Y., Jorgensen, E., Hartwieg, E., and Horvitz, H.R. (1999). The *Caenorhabditis elegans* gene unc-25 encodes glutamic acid decarboxylase and is required for synaptic transmission but not synaptic development. J. Neurosci. *19*, 539–548.

Kawano, T., Po, M.D., Gao, S., Leung, G., Ryu, W.S., and Zhen, M. (2011). An imbalancing act: gap junctions reduce the backward motor circuit activity to bias *C. elegans* for forward locomotion. Neuron *72*, 572–586.

Kiehn, O. (2006). Locomotor circuits in the mammalian spinal cord. Annu. Rev. Neurosci. *29*, 279–306.

Kiehn, O. (2011). Development and functional organization of spinal locomotor circuits. Curr. Opin. Neurobiol. *21*, 100–109.

Kristan, W.B., Jr., and Calabrese, R.L. (1976). Rhythmic swimming activity in neurones of the isolated nerve cord of the leech. J. Exp. Biol. *65*, 643–668.

Kunkel, M.T., Johnstone, D.B., Thomas, J.H., and Salkoff, L. (2000). Mutants of a temperature-sensitive two-P domain potassium channel. J. Neurosci. *20*, 7517–7524.

Leifer, A.M., Fang-Yen, C., Gershow, M., Alkema, M.J., and Samuel, A.D. (2011). Optogenetic manipulation of neural activity in freely moving *Caenorhabditis elegans*. Nat. Methods *8*, 147–152.

Li, W., Feng, Z., Sternberg, P.W., and Xu, X.Z. (2006). A *C. elegans* stretch receptor neuron revealed by a mechanosensitive TRP channel homologue. Nature *440*, 684–687.

Liewald, J.F., Brauner, M., Stephens, G.J., Bouhours, M., Schultheis, C., Zhen, M., and Gottschalk, A. (2008). Optogenetic analysis of synaptic function. Nat. Methods *5*, 895–902.

Liu, Q., Chen, B., Gaier, E., Joshi, J., and Wang, Z.W. (2006). Low conductance gap junctions mediate specific electrical coupling in body-wall muscle cells of *Caenorhabditis elegans*. J. Biol. Chem. *281*, 7881–7889.

Marder, E., and Calabrese, R.L. (1996). Principles of rhythmic motor pattern generation. Physiol. Rev. *76*, 687–717.

Marder, E., and Bucher, D. (2001). Central pattern generators and the control of rhythmic movements. Curr. Biol. *11*, R986–R996.

McClellan, A.D., and Jang, W. (1993). Mechanosensory inputs to the central pattern generators for locomotion in the lamprey spinal cord: resetting, entrainment, and computer modeling. J. Neurophysiol. *70*, 2442–2454.

McIntire, S.L., Jorgensen, E., Kaplan, J., and Horvitz, H.R. (1993). The GABAergic nervous system of *Caenorhabditis elegans*. Nature *364*, 337–341.

Mullins, O.J., Hackett, J.T., Buchanan, J.T., and Friesen, W.O. (2011). Neuronal control of swimming behavior: comparison of vertebrate and invertebrate model systems. Prog. Neurobiol. *93*, 244–269.

Pearce, R.A., and Friesen, W.O. (1984). Intersegmental coordination of leech swimming: comparison of in situ and isolated nerve cord activity with body wall movement. Brain Res. *299*, 363–366.

Pearson, K.G. (1995). Proprioceptive regulation of locomotion. Curr. Opin. Neurobiol. *5*, 786–791.

Pearson, K.G. (2004). Generating the walking gait: role of sensory feedback. Prog. Brain Res. *143*, 123–129.

Richmond, J.E., Davis, W.S., and Jorgensen, E.M. (1999). UNC-13 is required for synaptic vesicle fusion in *C. elegans*. Nat. Neurosci. *2*, 959–964.

Sauvage, P. (2007). Etude de la locomotion chez C. elegans et perturbations mecaniques du mouvement. PhD dissertation, Laboratoire Matiere et Systemes Compiexes (Paris, France: Universite Paris Diderot-Paris 7), p. 152.

Song, W., Onishi, M., Jan, L.Y., and Jan, Y.N. (2007). Peripheral multidendritic sensory neurons are necessary for rhythmic locomotion behavior in *Drosophila* larvae. Proc. Natl. Acad. Sci. USA *104*, 5199–5204.

Tavernarakis, N., Shreffler, W., Wang, S., and Driscoll, M. (1997). unc-8, a DEG/ENaC family member, encodes a subunit of a candidate mechanically gated channel that modulates *C. elegans* locomotion. Neuron *18*, 107–119.

Tian, L., Hires, S.A., Mao, T., Huber, D., Chiappe, M.E., Chalasani, S.H., Petreanu, L., Akerboom, J., McKinney, S.A., Schreiter, E.R., et al. (2009). Imaging neural activity in worms, flies and mice with improved GCaMP calcium indicators. Nat. Methods *6*, 875–881.

Wallén, P., and Williams, T.L. (1984). Fictive locomotion in the lamprey spinal cord in vitro compared with swimming in the intact and spinal animal. J. Physiol. *347*, 225–239.

White, J.G., Southgate, E., Thomson, J.N., and Brenner, S. (1976). The structure of the ventral nerve cord of *Caenorhabditis elegans*. Philos. Trans. R. Soc. Lond. B Biol. Sci. *275*, 327–348.

White, J.G., Southgate, E., Thomson, J.N., and Brenner, S. (1986). The structure of the nervous system of the nematode *Caenorhabditis elegans*. Philos. Trans. R. Soc. Lond. B Biol. Sci. *314*, 1–340.

Yu, X., and Friesen, W.O. (2004). Entrainment of leech swimming activity by the ventral stretch receptor. J. Comp. Physiol. A Neuroethol. Sens. Neural Behav. Physiol. *190*, 939–949.

Yu, X.T., Nguyen, B., and Friesen, W.O. (1999). Sensory feedback can coordinate the swimming activity of the leech. J. Neurosci. *19*, 4634–4643.

Zhang, F., Wang, L.P., Brauner, M., Liewald, J.F., Kay, K., Watzke, N., Wood, P.G., Bamberg, E., Nagel, G., Gottschalk, A., and Deisseroth, K. (2007). Multimodal fast optical interrogation of neural circuitry. Nature *446*, 633–639.

Zheng, Y., Brockie, P.J., Mellem, J.E., Madsen, D.M., and Maricq, A.V. (1999). Neuronal control of locomotion in *C. elegans* is modified by a dominant mutation in the GLR-1 ionotropic glutamate receptor. Neuron *24*, 347–361.